Vol. 47, No. 2 (2025) 313-325, DOI: 10.24874/ti.1896.02.25.04

Tribology in Industry

www.tribology.rs

RESEARCH

Optimizing Milling Parameters and Halloysite Nanotube Concentration to Enhance Surface Quality and Reduce Energy Consumption

Laura Peña-Parás[a,*], Martha Rodríguez-Villalobos[b], Demófilo Maldonado-Cortés[a], Jaime A. González-García[a], Mónica Herrera-Maldonado[a], Gabriela Trousselle-Strozzi[a], Oscar E. Montemayor[a], Ángel G. Romero-Cantú[a], Daniel I. Quintanilla-Correa[a]

[a]*Universidad de Monterrey, Mechanical and Electronic Engineering Department, Av. Morones Prieto 4500 Pte., San Pedro Garza García, N. L. 66238, Mexico,*
[b]*Universidad de Monterrey, Physics and Mathematics Department, Av. Morones Prieto 4500 Pte., San Pedro Garza García, N. L. 66238, Mexico.*

Keywords:

Optimization
Milling process
Halloysite clay nanotubes
Cutting fluids

* Corresponding author:

Laura Peña Parás
E-mail: laura.pena@udem.edu

Received: 13 February 2025
Revised: 17 March 2025
Accepted: 22 April 2025

A B S T R A C T

Numerous studies have focused on determining the optimal machining parameters for various steels, aiming to reduce both energy consumption and the average surface roughness (R_a) of manufactured parts. In this study, a Computer Numerical Control (CNC) milling machine was used to machine AISI 4340 steel bars with varying input parameters, including spindle speed (rpm), depth of cut (in), feed rate (in/min), and HNT concentration (wt.%). A design of experiments based on a three-level Box-Behnken approach was employed to identify the optimal values for these milling parameters. Spindle load (SL) and surface roughness (R_a) of the milled steel bars were measured after each test. A Response Surface Methodology (RSM) model was developed to optimize the input variables, which indicated that the optimal HNT concentration ranged from 0.11 to 0.17 wt.%. The regression models for R_a and SL demonstrated determination coefficients (R^2) of 61.65% and 81.64%, respectively. The optimal values were a spindle speed of 920 rpm, a depth of cut of 0.02 in, a feed rate of 10.5 in/min, and an HNT concentration of 0.12 wt.%. The predicted values were 682 nm for R_a and 1.5 kW for SL, while confirmatory experiments resulted in R_a and SL values of 764 nm and 1.6 kW, respectively. These findings show that optimizing machining parameters, combined with the addition of HNTs to cutting fluids, can enhance the surface roughness of milled parts while reducing energy consumption. This optimization provides significant benefits, including reduced production costs, improved part quality, and a lower carbon footprint in the manufacturing process.

1. INTRODUCTION

Energy consumption has emerged as a significant challenge in the metal-mechanic industry [1-2]. Therefore many efforts are constantly being made to increase the productivity and efficiency of metalworking processes. Friction and wear between contacting surfaces during these processes not only reduce the lifespan of tools and components but also have a considerable impact on the consumption of natural resources [1].

Machining, the process of removing material from a workpiece to achieve different shapes and dimensions, is a fundamental aspect of the manufacturing industry. Over the years, researchers have focused on advancing various techniques and innovations aimed at enhancing the efficiency, precision, and overall performance of machining processes. One of these solutions has been the addition of nanoparticles (NPs) to the cutting fluids [3-5]. Thanks to their tribological enhancement mechanisms NPs have demonstrated improvements in the performance of lubricants [3,6,7], where the optimal NP concentration may vary according to the nature of the cutting fluid, material to be machined, and the specific processing conditions of each material. For example, adding NPs of SiO_2, TiO_2 and Ag to process fluids reduced the Coefficient of Friction (COF) and wear depth by up to 8.9% and 52.1%, respectively [8]. Hexagonal boron nitride (hBN) NPs dispersed in jatropha oil reduced friction and wear by 76% and 24%, respectively [9]. Similarly, vegetable oils such as coconut, sesame, and canola oils reinforced with molybdenum disulphide (MoS_2) have shown performance improvements. García et al. [10] added TiO_2 NPs to a grinding lubricant for producing slitting knives reducing surface roughness of the manufactured product. Finally, tool life was prolonged by 40.17% by adding Al_2O_3 NPs to a coconut bio-based oil, which yielded lower values of cutting forces, spindle power, specific cutting energy and surface roughness when machining Inconel 718 alloy [11].

Halloysite clay nanotubes (HNTs) have recently gained attention as green lubricant additives, demonstrating significant improvements in tribo-characteristics in laboratory studies [12-14]. These NPs, with a chemical formula of $Al_2Si_2O_5(OH)_4 \bullet 2H_2O$, have diameters of less than 100 nm, and a length of approximately 500 nm to several microns [15]. Due to their straight and individual particle structure, their dispersion is relatively simple. HNTs also exhibit excellent mechanical properties, with a Young's modulus experimentally measured of ~140 GPa [16]. Additionally, they are non-toxic, inexpensive, biocompatible, environmentally friendly, and their production exceeds thousands of tons per year [15]. Zhang et al. [14] found that HNTs may form an anti-wear tribofilm under abrasive conditions. In another study, anti-wear and friction reducing properties of mineral oil and synthetic fluids were enhanced with 0.1 wt.% HNTs [12]. Similarly, block-on-ring tests performed with HNTs dispersed in a polymeric lubricant showed a reduction in COF and wear volume loss by approximately 70%, compared to the unfilled lubricant. The same nanolubricant increased load carrying capacity thanks to the formation of a tribofilm and by reducing the contact area between moving components [13]. Furthermore, Maldonado et al. [17] incorporated HNTs into the lubricant for the ball screw component of a CNC lathe, resulting in a 38% improvement in wear resistance.

The surface quality of milled parts is also a critical factor, as it directly influences the product's appearance, functionality, and overall reliability [18,19]. In this context, Karolczak et al. [19] increased turning productivity of Ti6Al4V without sacrificing surface quality through Minimum Quantity Lubrication (MQL). However, other approaches, such as the optimization of milling parameters, have been explored for the metalworking industry, particularly to promote cleaner production. The objective is to produce parts in the shortest time possible while reducing energy consumption, enhancing surface quality, and improving overall efficiency [20]. Significant efforts have been made to identify the optimal parameters that allow equipment to operate efficiently while preventing damage to cutting tools [21,22]. In addition to the complexity of the optimization process, it is essential to consider the material being machined, as it often plays a critical role in determining the characteristics and performance of the final part [23]. Optimization may focus on various output variables, and is typically performed using statistical tools or optimization algorithms [24]. For example, multi-objective optimization tools of the machining parameters for 38CrMoAl led to tool wear reductions of up to 33% [25]. Kuntoglu et al. [23] investigated the optimization of machining parameters for AISI 1050 steel and

obtained reductions in tool wear and cutting forces of up to 33% and 24%, respectively. In another study, reductions of 10.6% in the frictional torque were obtained using optimization techniques when milling AISI 4130 steel, also lowering the carbon footprint of the process [26]. The Taguchi optimization method has been used to lower tool wear by 32% when machining 17-4 PH stainless steel [27], and for lowering cutting forces, cutting temperature, and surface roughness when milling Al 6061-T6 in combination with SiO_2 nano-additives [28]. Furthermore, Ronoh et al. [29] used a Taguchi orthogonal array to evaluate the effects of cutting fluids, cooling methods, and grinding depths on the surface roughness of Ti6Al4V. Optimal surface roughness was obtained with a sunflower oil fluid, MQL, and a grinding depth of 0.005 mm.

The Box-Behnken design is widely used for efficiently estimating main effects and interactions with fewer experimental runs, making it ideal when time or resources are limited. It does not rely on factorial designs, offering a more cost-effective approach. By predicting first- and second-order coefficients with fewer design points, it reduces the need for extensive experimentation. While its coverage of the nonlinear design space is limited, it is generally considered more efficient than other designs, such as three-level fractional factorial designs. Additionally, the design is rotatable, requires three levels per factor, and can adapt to a full quadratic model for response surface analysis [30,31]. For example, Mwangi et al. [18] employed the Box-Behnken design in Response Surface Methodology (RSM) to evaluate surface quality and productivity in the milling of Cu-Be C17200 using MQL. They found that surface quality improved with increasing cutting depth, while lower surface roughness values were achieved at reduced cutting depths. The Box-Behnken design approach has also been used in several studies that optimized machining parameters and NP additives [18,21,32-34] which take into consideration the effect of different parameters simultaneously on the response variables. In a previous study by our group using this approach [21], montmorillonite (MMT) clay NPs, another environmentally friendly additive, were added to the cutting fluid for the milling of an AISI 1018 (with a hardness of 71 HRB). Milling parameters such as of cutting speed, depth of cut, and feed rate were also optimized, resulting in lower Spindle Loads (SL) and surface roughness.

AISI 4340 steel is widely employed for aerospace, aircraft, powertrain applications, among others [35]. In this study, we investigated the milling of AISI 4340 steel to produce steel ring parts used in aerospace and oil and gas applications. The objective was to optimize the milling parameters for a manufacturing company. The milling parameters were adjusted to reduce the spindle load (SL) in kW, which is related to the energy consumption of the process, while ensuring that the target surface roughness, in terms of R_a, remained at approximately 0.8 microns (800 nm), as required for the client's specifications. Milling of the steel bars was carried out on CNC milling equipment with different combinations of spindle speeds, depth of cuts, feed rates and concentration of NPs of HNTs in the lubricant.

2. EXPERIMENT DETAILS

2.1 Material selection

A water-soluble synthetic lubricant, Bio Syntek HD by Lufhissa (Mexico), was used at a concentration of 7.6% for the milling experiments. HNTs, with diameters ranging from 30 to 70 nm and lengths from 1 to 3 μm, were obtained from Sigma-Aldrich (Germany). HNTs were weighed on a scale and dispersed at concentrations of 0.1 and 0.2 wt.% via sonication for 5 min with a Cole-Parmer ultrasonic processor model 500 W (United States) with an operating frequency of 20 kHz. The concentrations were selected based on previous experiments conducted by our group [36,37].

2.2 Milling tests

A CNC machine, model VF2, manufactured by HAAS (United States) (Fig. 1a) was used to perform the milling experiments. This CNC is a vertical machining center with workbench dimensions of 76 x 40 x 50 cm, an output power of 22.4 kW, and coolant tank capacity of 208 L. Round bars of AISI 4340 steel, with hardness of 95 HRB (Carpenter, United States) (Fig. 1b) with a diameter of 10.16 cm and hardness of 95 HRB were used for the milling experiments. Cemented carbide cutting tools coated with MT-TiCN + Al_2O_3 + TiN were supplied by Korloy (South Korea) (Fig. 1c). For each test, two inserts were mounted on the face shell mill.

A CNC program was designed to allow for the machining of the AISI 4340 steel bars in three passes. This program permitted the modification of the input machining parameters, which were: depth of cut (in), feed rate (in/min), spindle speed (rpm), and HNT wt.% in the lubricant. The outputs obtained were: SL (related to energy consumption, kW), recorded from the controller electronic display (Fig. 1a), and average surface roughness of the workpiece (R_a, nm), measured with a microscope Alicona, model IF-EdgeMaster (Austria), a focus variation 3D surface measurement system. This microscope is an advanced optical technology designed for high-resolution 3D surface measurements. It employs precision optics with adjustable lenses and vertical scanning to capture both topographical and color data, enabling efficient measurement of surface form and roughness in a single process. For each steel plate, three to five measurements were taken, and their averages were reported for each test.

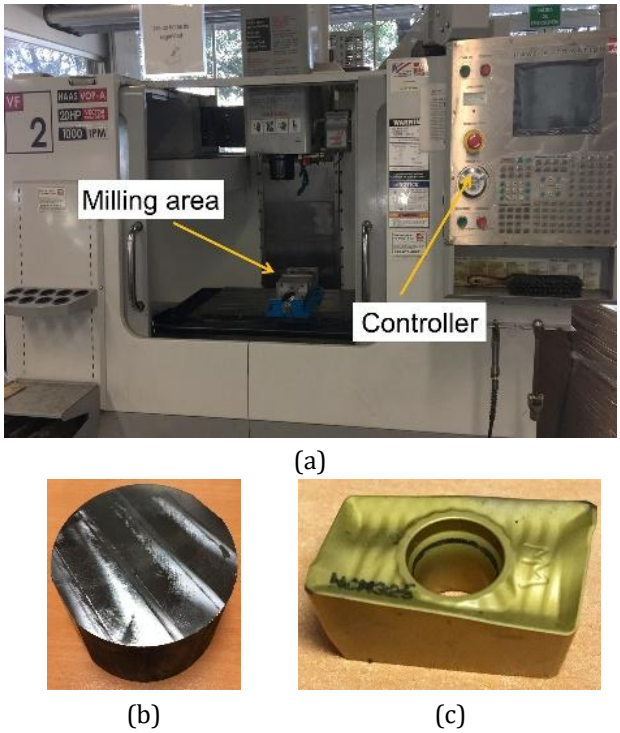

(a)

(b)

(c)

Fig. 1. (a) HAAS VF2 CNC Machine, (b) AISI 4340 steel bar, (c) cutting insert.

2.3 Design of experiments

A Box-Behnken experimental design was implemented, considering three different levels (low, medium, and high) for each input variable: spindle speed (and the corresponding cutting speed), depth of cut, feed rate, and HNT wt.%. Table 1 shows the values of the three levels for each input variable. The values for the milling parameters were based on the cutting insert supplier recommendations for the selected material, as well as previous studies by our group. The levels for HNT wt.% were determined based on previous studies conducted by our group [36,37]. The duration of each experiment depended on the feed rate and was set to 10 minutes, 20 minutes, and 30 minutes for feed rates of 15 in/min, 10 in/min, and 5 in/min, respectively. Table 2 shows the 27 combinations obtained from the Box-Behnken design; three tests were run for each combination resulting in a total of 81 tests.

Table 1. CNC Machining parameters and HNT concentrations.

Level	Spindle speed [rpm] (*Cutting speed [ft/min]*)	Feed rate [in/min]	Depth of cut [in]	HNT [wt.%]
1	400 (*313*)	5	0.01	0
2	800 (*627*)	10	0.02	0.1
3	1200 (*929*)	15	0.03	0.2

Table 2. Input parameters for the design of experiments.

	Input variables			
Run	Spindle Speed [rpm]	Feed rate [in/min]	Depth of cut [in]	HNTs [wt.%]
1	400	10	0.02	0
2	800	5	0.02	0
3	800	10	0.01	0
4	800	10	0.03	0
5	800	15	0.02	0
6	1200	10	0.02	0
7	400	5	0.02	0.1
8	400	10	0.01	0.1
9	400	10	0.03	0.1
10	400	15	0.02	0.1
11	800	5	0.01	0.1
12	800	5	0.03	0.1
13	800	10	0.02	0.1
14	800	10	0.02	0.1
15	800	10	0.02	0.1
16	800	15	0.01	0.1
17	800	15	0.03	0.1

18	1200	5	0.02	0.1
19	1200	10	0.01	0.1
20	1200	10	0.03	0.1
21	1200	15	0.02	0.1
22	400	10	0.02	0.2
23	800	5	0.02	0.2
24	800	10	0.01	0.2
25	800	10	0.03	0.2
26	800	15	0.02	0.2
27	1200	10	0.02	0.2

The average values for each of the 27 tests were calculated for the response variables of R_a and SL, and their results are shown in Table 3.

Table 3. Average results of the output variables for each of the 27 combinations.

	Output variables	
Run	***Ra* [nm]**	**SL [kW]**
1	1,037.253	2.700
2	667.500	1.667
3	939.197	1.400
4	723.827	1.967
5	674.136	2.233
6	752.334	2.500
7	660.772	1.833
8	601.177	1.600
9	842.782	3.067
10	890.497	3.333
11	559.655	1.367
12	735.905	1.500
13	701.001	1.567
14	676.495	1.367
15	731.263	1.600
16	575.561	1.567
17	732.512	1.967
18	414.536	1.167
19	669.740	2.000
20	554.115	1.733
21	643.006	1.600
22	693.970	2.233
23	714.589	1.433
24	844.733	1.567
25	654.000	2.433
26	769.975	1.767
27	675.544	2.367

After obtaining the data, two models were estimated. The first model, in the form of quadratic polynomials, was developed using RSM, as shown in Eq. (1). To determine the optimal parameters, the second model was estimated, as shown in Eq. (2).

$$Y_i = \delta_0 + \sum_{i=1}^{4} \delta_i X_i + \sum_{i=1}^{4} \sum_{j=1}^{4} \delta_{ij} X_i X_j + \sum_{i=1}^{4} \delta_{ii} X_i^2 + \varepsilon_i \quad (1)$$

$$Y_i = \alpha_{i0} + \alpha_{i1} X_i + \alpha_{i2} X_i^2 + \mathcal{E}_i \quad (2)$$

In Model 1, presented in Eq. (1), δ_0 is the constant term, δ_i is the first-order coefficient, δ_{ij} is the second-order coefficient (when $i=j$) and the interaction coefficient (when $i \neq j$). The X variables represent the input variables of spindle speed, depth of cut, feed rate, and HNT wt.% and ε is the error. All analyses were carried out with MINITAB at a significance level of 0.05. Model 2 (Eq. (2)) was employed to determine the optimized levels for the input variables. The first-order conditions were applied to identify the optimized levels of the input variables represented in the model, where α_{i0} is the intercept coefficient, α_{i1} is the linear coefficient and α_{i2} is the quadratic coefficient.

3. RESULTS AND DISCUSSION

3.1. Results of milling experiments

Contour plots were created with the data from Table 2 and Table 3 in order to visualize the effect of adding HNTs in combination with each of the milling parameters, as shown in Fig. 2 and Fig. 3. In these figures, the x-axis represents the HNT wt.%, while the y-axis corresponds to the milling parameters, including spindle speed, depth of cut, or feed rate, respectively.

Fig. 2 presents the contour maps for SL, showing the interaction of milling parameters (spindle speed, depth of cut, and feed rate) with respect to HNT (or NP) concentration. From these plots, it can be observed that, in general, middle concentrations of HNTs are able to provide lower SL values. Fig. 2a shows the combinations of spindle speeds and NP concentrations that result in the lowest SL (kW), considering a fixed feed rate of 10 in/min and a depth of cut of 0.02 in. The dark blue region corresponds to medium HNT

levels (around 0.10 wt.%) with a spindle speed range between 800-1000 rpm. In Fig. 2b, the light green region shows the lowest SL levels with combinations of depth of cut (between 0.010 and 0.015 in) and NP (0.6-0.18 wt.%) at a fixed spindle speed of 800 rpm and a feed rate of 10 in/min. Fig. 2c presents the combinations of feed rate and NP with a fixed spindle speed of 800 rpm and a depth of cut of 0.10 in. The dark blue area represents the region with the lowest SL levels, corresponding to a feed rate of around 5 in/min and NP levels between 0.08-0.12 wt.%.

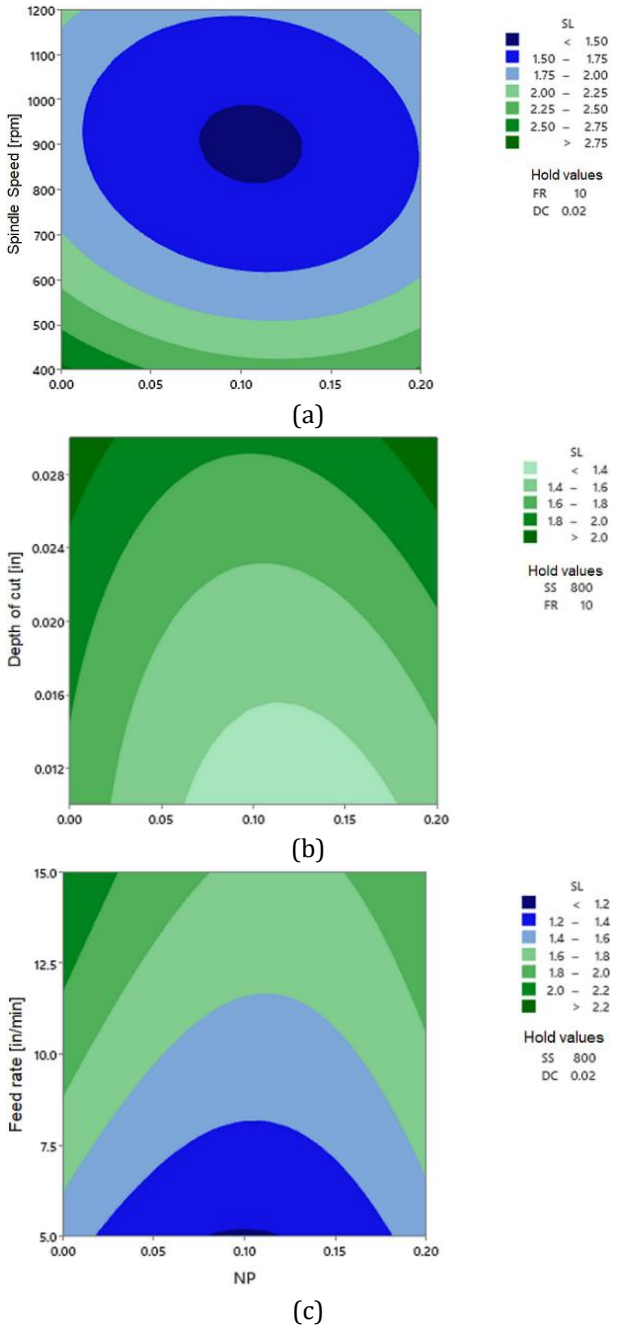

Fig. 2. Contour plots for SL for: (a) spindle speed, (b) depth of cut, and (c) feed rate vs. nanoparticle concentration.

Fig. 3 presents contour plots for surface roughness with the same fixed values as those in Fig. 2, demonstrating the interactive effects of the independent variables on this response.

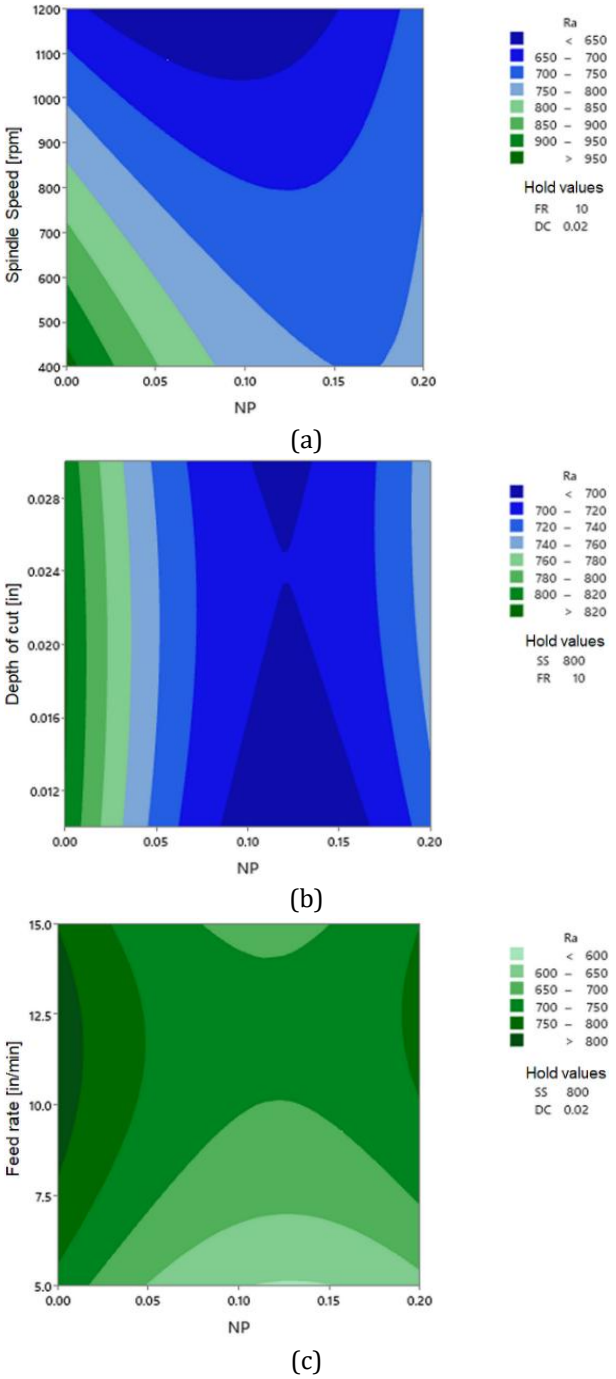

Fig. 3. Contour plots for surface roughness (R_a) for: (a) spindle speed, (b) depth of cut, and (c) feed rate vs. nanoparticle concentration.

In Fig. 3a, the dark blue area with a SL higher than 1050 rpm and NP levels between 0.1-0.15 wt.% generates the lowest R_a. In Fig. 3b, the NP levels corresponding to the lowest surface roughness are between 0.09 and 0.17 wt.%. Similar to the SL

variable (Fig. 2c), the feed rate and NP levels that fall within the light green area with the lowest surface roughness are around 5 in/min and NP between 0.11-0.15 wt.%. Fig. 3c also shows that middle concentrations of HNTs allow for higher feed rates, improving the efficiency of the manufacturing process. Therefore, HNTs are able to reduce the contact between the cutting inserts and the steel bars, reducing friction and allowing for smoother surfaces.

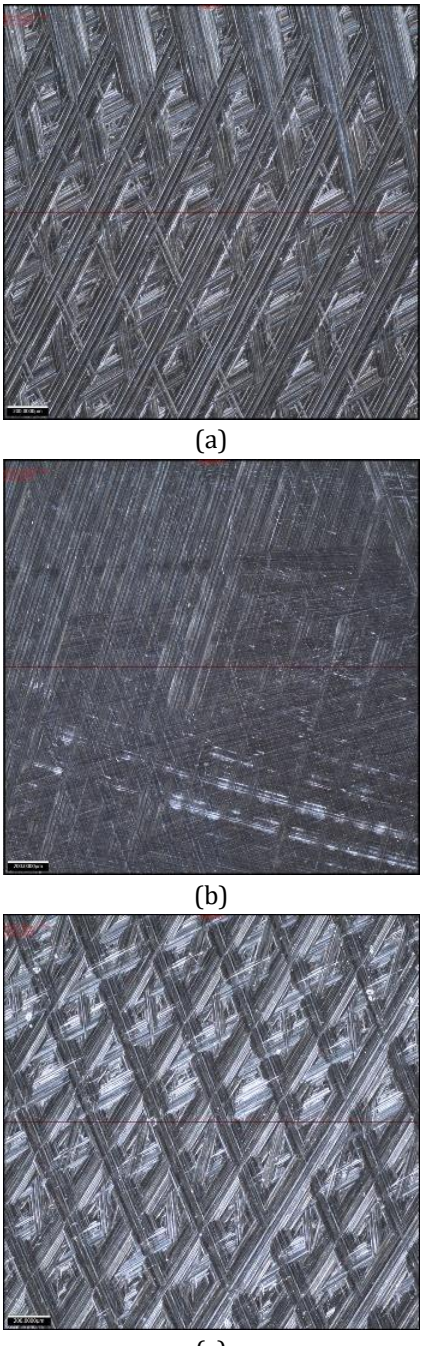

(a)

(b)

(c)

Fig. 4. Milled AISI 4340 steel workpieces under varying conditions: (a) 0 wt.% HNT, 800 rpm, 0.03 in, 10 in/min, (b) 0.1 wt.% HNT, 1200 rpm, 0.02 in, 5 in/min (c) 0.2 wt.% HNT, 800 rpm, 0.03 in, 10 in/min.

Images and roughness profiles of selected milled AISI 4340 steel parts obtained through focus-variation microscopy, under different conditions of HNT concentration (0, 0.1 and 0.2 wt.%) and spindle speed, depth of cut, and feed rate, are shown in Fig. 4 and Fig. 5. These specific combinations were selected from the 81 individual runs (rather than the average values) to examine the effect of HNT addition on the milled surface quality, under milling conditions of spindle speed, depth of cut, and feed rate that were as similar as possible. Smoother surfaces with lower R_a values can be observed with the combination of HNT concentration and milling parameters of 0.1 wt.% HNT, 1200 rpm, 0.02 in, 5 in/min (Fig. 4b and Fig. 5b), compared to 0 wt.% HNT, 800 rpm, 0.03 in, 10 in/min (Fig. 4a and Fig. 5a) and 0.2 wt.% HNT, 800 rpm, 0.03 in, 10 in/min (Fig. 4c and Fig. 5c).

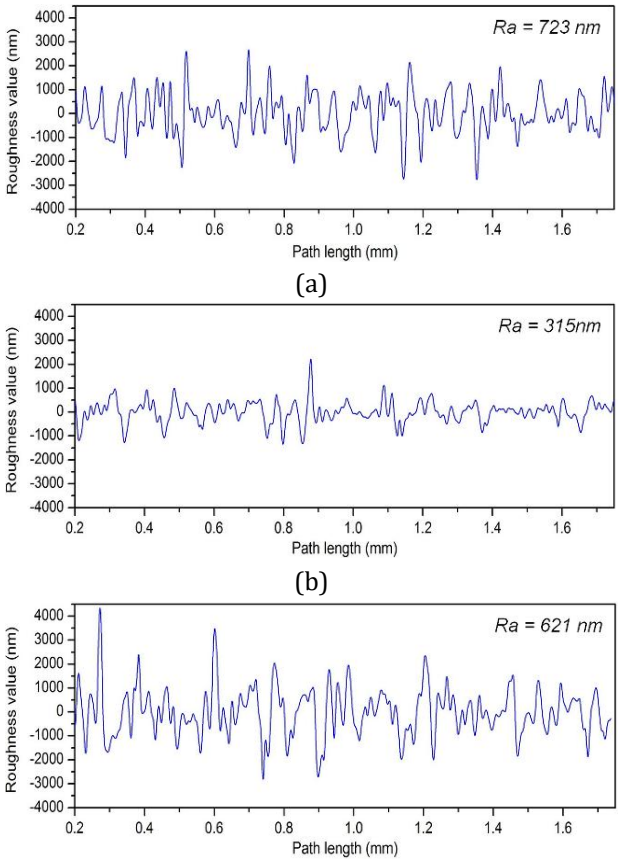

(a)

(b)

(c)

Fig. 5. Roughness profiles and R_a of milled steel workpieces under varying conditions: (a) 0 wt.% HNT, 800 rpm, 0.03 in, 10 in/min, (b) 0.1 wt.% HNT, 1200 rpm, 0.02 in, 5 in/min, (c) 0.2 wt.% HNT, 800 rpm, 0.03 in, 10 in/min.

The improvements in R_a observed with HNTs can be attributed to their load-bearing effect, as

demonstrated in previous studies by our group [13,36,37]. This effect helps reduce contact between the tool and the workpiece, resulting in a smoother surface. It should be noted that while typical R_a values for milled parts range from 800 – 6300 nm [38], the specific requirements for this study were R_a values of ~800 nm, as these are the product specifications set by the manufacturing company. Additionally, a lower spindle load is preferred for improved process efficiency.

It is further proposed that HNTs reduce the area of contact between the cutting insert and the workpiece (Fig. 6), and provide a load-bearing effect due to their high mechanical properties (E = 140 GPa, [16]) thus reducing SL and surface roughness.

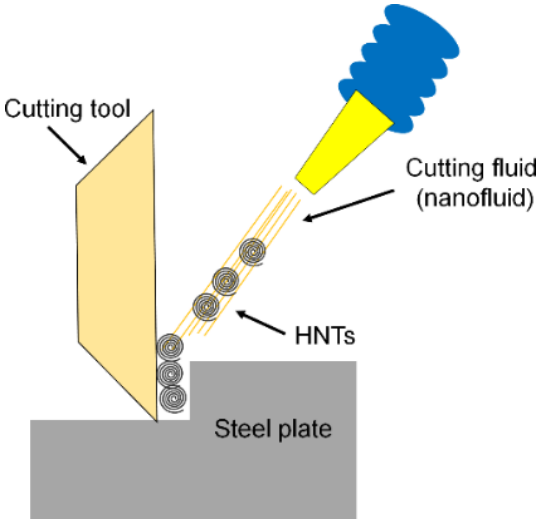

Fig. 6. Load-bearing effect of the HNTs between the cutting tool and the work piece.

These findings highlight the significance of incorporating HNTs into the cutting fluid and optimizing milling parameters for enhanced performance. Based on the results of this study, it can be concluded that the addition of HNTs to cutting fluids is beneficial for milling processes, allowing for faster processing of steel parts, and improving the efficiency of the process.

3.2. Statistical analyses and optimization of milling parameters

The regression models for surface roughness of milled steel bars and SL were estimated and are shown in Eq. (3) and (4), respectively. In these equations *S*, *F*, *D* and *HNT* represent the spindle speed, feed rate, depth of cut, and HNT wt.%, respectively. The coefficients of determination (R^2) for Eq. 3 and Eq. 4 were 61.65% and 81.64% respectively. Table 4 and Table 5 show the ANOVA results of the models for R_a and SL, respectively. As part of the assumptions of the RSM model, the Anderson-Darling test was performed to assess the normality of the errors. For R_a, the p-value was 0.362, and for SL, it was 0.694, indicating that in both cases, the errors follow a normal distribution.

$$R_a = 409 + 0.134\,S + 53.4\,F + 21365\,D - 3716\,HNT - 0.000040\,S^2 - 2.24\,F^2 - 67809\,D^2 + 8245\,HNT^2 - 0.0002\,S*F - 22.3\,S*D + 1.67\,S*HNT - 96\,F*D + 24\,F*HNT + 6159\,D*HNT \quad (3)$$

Table 4. ANOVA results of the model for R_a.

Source	Sum of Squares	DF	Mean Squares	F	P-Value	
Model	256879	14	18348.5	1.38	0.292	
S	86221	1	86221.0	6.52	0.017	*
F	23650	1	23650.0	1.50	0.231	
D	235	1	234.8	0.01	0.906	
HNT	16239	1	16239.0	1.01	0.324	
*S*F*	9412	1	9412.0	0.58	0.454	
*S*D*	52232	1	52232.0	3.58	0.070	
*S*HNT*	41696	1	41696.0	2.78	0.108	
*F*D*	13278	1	13278.0	0.82	0.373	
*F*HNT*	1419	1	1419.0	0.09	0.772	
*D*HNT*	10129	1	10129.0	0.62	0.437	
S^2	86186	1	86186.0	6.52	0.017	*
F^2	13948	1	13948.0	0.87	0.361	
D^2	99	1	99.5	0.01	0.939	
HNT^2	1060	1	1060.0	0.06	0.803	
Residual	159827	12	13318.9			
Lack of Fit	158321	10	15832.1	21.04	0.046	
Pure Error	1505	2	752.6			
Cor Total	416706	26				
*Statistically significant at the 0.05 level						

$$SL = 1.31 - 0.00294\,S + 0.178\,F + 69.4\,D - 8.94\,HNT + 0.000003\,S^2 - 0.00139\,F^2 + 569\,D^2 + 31.9\,HNT^2 - 0.000133\,S*F - 0.1083\,S*D + 0.00208\,S*HNT + 1.33\,F*D - 0.117\,F*HNT + 75\,D*HNT \quad (4)$$

Table 5. ANOVA results of the model for SL.

Source	Sum of Squares	DF	Mean Squares	F	P-Value	
Model	6.2038	14	0.4431	3.81	0.013	*
S	0.9633	1	0.9633	3.63	0.068	
F	1.0208	1	1.0208	3.88	0.060	
D	0.8357	1	0.8357	3.09	0.091	
HNT	0.0370	1	0.0370	0.12	0.729	
*S*F*	0.0075	1	0.0075	0.02	0.876	
*S*D*	0.0484	1	0.0484	0.16	0.692	

*S*HNT*	0.3025	1	0.3025	1.04	0.318	
*F*D*	1.8496	1	1.8496	8.04	0.009	*
*F*HNT*	0.0584	1	0.0584	0.19	0.664	
*D*HNT*	0.0711	1	0.0711	0.24	0.631	
S^2	0.5413	1	0.5413	1.92	0.178	
F^2	0.7902	1	0.7902	2.90	0.101	
D^2	0.7164	1	0.7164	2.60	0.119	
HNT^2	0.0000	1	0.0000	0.00	0.994	
Residual	1.3953	12	0.1163			
Lack of Fit	1.3634	10	0.1363	8.56	0.109	
Pure Error	0.0319	2	0.0159			
Cor Total	7.5991	26				
*Statistically significant at the 0.05 level						

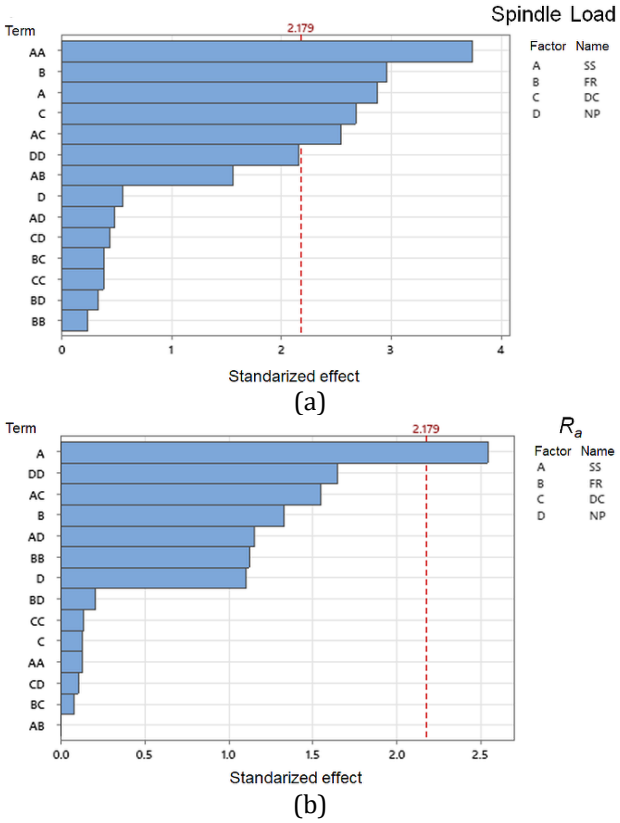

Fig. 7. Pareto charts of standardized effects for (a) SL and (b) R_a.

Fig. 7 shows the Pareto diagram used to analyze the magnitude of the effects of the factors on R_a and SL. For SL (Fig. 7a), all factors were initially considered significant. The standardized effects indicate that spindle speed has the most significant impact, being important at both the linear and quadratic levels, followed by feed rate and depth of cut. Additionally, there is an interaction effect between spindle speed and depth of cut. However, due to variability in the error, the factors were not found to be significant in the ANOVA for SL. In the case of R_a (Fig. 7b), it was observed that the only significant factor was spindle speed. Therefore, a univariate quadratic model was adopted to focus on the most influential parameter. This simplified approach aligns with the data and supports clearer and more robust optimization.

As mentioned earlier, Model 2 (Eq. (2)) was used to determine the optimized input variable levels by applying first-order conditions. These conditions are obtained by setting the first derivative equal to zero, which indicates a zero slope and a change in the function's trend. The optimal values are determined using this approach, with the model allowing analysis of how each input parameter affects the response variables: $X_i^* = -\alpha_{i1}/2\alpha_{i2}$. Table 6 shows the linear and quadratic coefficients for Model 2, where the factors of spindle speed, feed rate, depth of cut, and HNT wt.% are represented with the variables in *S*, *F*, *D*, and *HNT*, respectively.

Table 6. Coefficients of Model 2.

Variable	**Coefficients of Model 2.**			
	Coefficient for R_a		Coefficient for SL	
	α_1	α_2	α_1	α_2
S	-0.108	-0.000065	-0.00555	0.000003
F	64.8	-2.8	0.235	-0.00882
D	4745	-107577	70.6	-1106
HNT	-2294	9632	-4.64	20.4

The optimized values for the milling parameters of spindle speed, depth of cut, feed rate, and HNT concentration in the cutting fluid obtained from the coefficients in Model 2 (Eq. (2)), and presented in Table 6, are shown in Table 7. For example, for the input variable *F* in relation to R_a, the optimal value is calculated as $X_i^* = -\alpha_{i1}/2\alpha_{i2} = -(64.8)/(2*(2.8))=11.57$ in/min. The same procedure was applied to determine all the optimal values presented in Table 7. Similar optimized HNT concentrations (0.11 and 0.17 wt.%) were obtained for both SL and surface roughness, and these input parameters are within the optimal range of the contour plots in Fig. 3 and Fig. 2. As previously discussed, for practical milling applications like this one, R_a values around 800 nm are acceptable. Moreover, as long as the values remain within the acceptable range specified by the client for the required product, a lower spindle load is preferred to enhance process efficiency.

Table 7. Optimized input parameters.

Response parameters	Optimized input parameters			
	Spindle speed [S, rpm]	Depth of cut [D, in]	Feed rate [F, in/min]	HNT [wt.%]
Spindle Load, (SL, kW)	925	0.0220	13.32	0.11
Surface roughness (R_a, nm)	*	0.0319	11.57	0.17

*Note: For R_a the estimated parameter was not the minimal.

Considering the optimized results in Table 7 and the optimal ranges shown in Fig. 2 and Fig. 3, the following parameters were selected for the validation run: spindle speed of 920 rpm, depth of cut of 0.02 in, feed rate of 10.5 in/min, and HNT concentration of 0.12 wt.%.

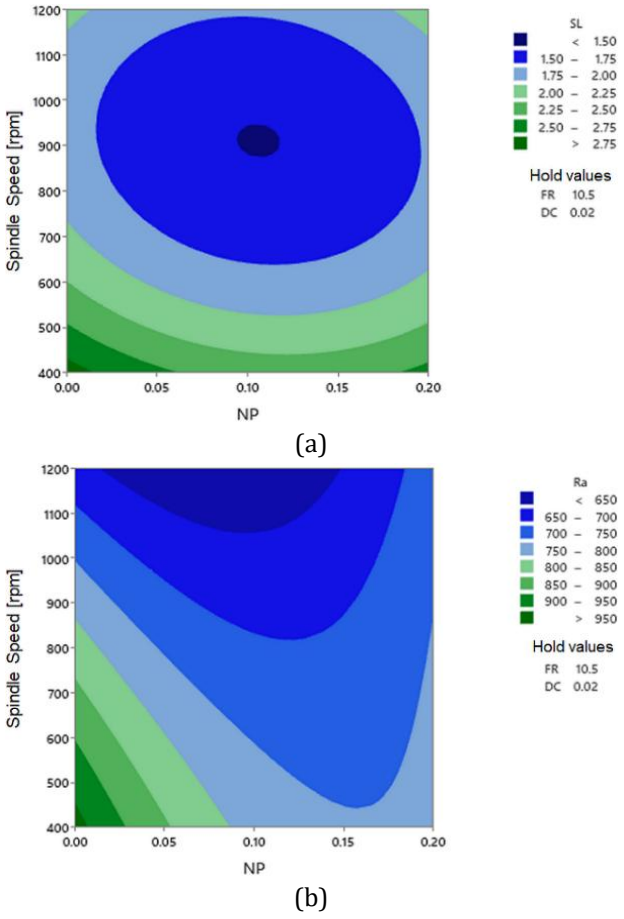

Fig. 8. Contour maps of (a) SL and (b) R_a showing spindle speeds and NP concentration with optimal values of feed rate and depth of cut.

Fig. 8 shows the contour plots of the optimized values. Fig. 8a illustrates that, with the optimal values, the dark blue area corresponds to R_a levels between 650-700 nm. Fig. 8b presents the combinations of spindle speed and NP, with the fixed optimal values for feed rate and depth of cut. It is observed that with a spindle speed of 920 rpm and 0.12 wt.% NP, the resulting SL value falls within the dark blue area.

The predicted results using these parameters, according to the regression models in Eq. (3) and Eq. (4), were a surface roughness (R_a) of 682 nm and a SL of 1.5 kW, with prediction errors of 63.422 and 0.187, respectively. In contrast, for the same milling parameters (920 rpm, 0.02 in depth of cut, and 10.5 in/min feed rate) without the addition of HNTs, the predicted results were a R_a of 779 nm and a SL of 1.85 kW, with prediction errors of 61.633 and 0.182, respectively. These comparisons suggest that the addition of HNTs may contribute to improvements in both surface roughness and SL, as indicated by the regression models.

Confirmatory milling experiments with the optimized input parameters of spindle speed of 920 rpm, depth of cut of 0.02 in, feed rate of 10.5 in/min, and HNT concentration of 0.12 wt.% were performed in triplicate and average values were calculated. The experimental values were 1.6 kW for SL and 764 nm for R_a, respectively. The results from the experimental and predicted values show a reasonable agreement, with percentage differences of 12.02% for R_a and 6.6% for SL. Therefore, the overall trends and predictions suggest that the model offers valuable insights into the milling process. Future work will focus on refining the model, particularly to improve accuracy for SL, and optimizing process parameters for better performance. The findings emphasize the potential of the developed model to guide more efficient milling operations, though further validation and adjustments are necessary for more precise predictions. To enhance the regression models presented in Eq. (3) and Eq. (4), future studies should incorporate additional parameters, such as lubricant flow, fluid viscosity, equipment vibration, and other relevant factors.

Fig. 9 presents the fitted means of the response variables, comparing the effect of no HNTs versus the optimized concentration (0.12 wt.%) based on the experimental results.

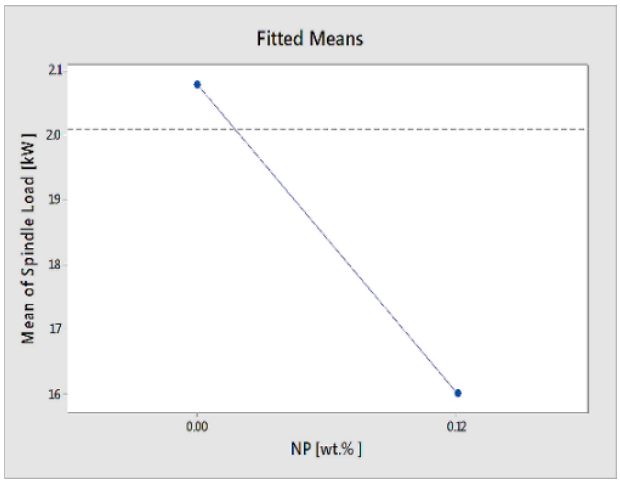

(a)

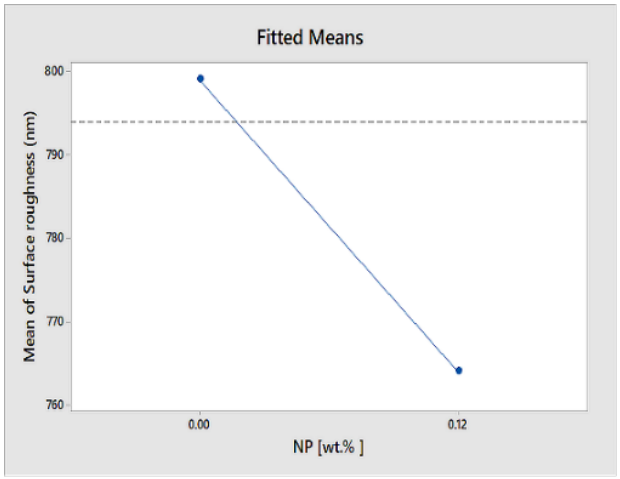

(b)

Fig. 9. Fitted means of response variables (a) Spindle Load and (b) Surface Roughness comparing HNT values of 0 wt.% and 0.12 wt.%.

From these plots, it can be observed that both the average R_a and SL show improvement with the addition of HNTs, and these improvements are statistically significant. Therefore, the results from this study can be used by manufacturing companies to tailor the milling parameters of AISI 4340 and HNT concentration in the milling fluid to target specific power consumption (SL) values and the desired surface roughness.

4. CONCLUSION

This study focused on the optimization of milling parameters for AISI 4340 steel and HNT concentration in the cutting fluid using RSM, with the goal of minimizing spindle load (or power consumption) while achieving a surface roughness value typical for milled parts and meeting the manufacturing company's requirements of 800 nm (0.8 µm). The results demonstrated that HNTs provided a load-bearing effect. The optimization of input parameters for both SL and R_a revealed that the optimal HNT concentration in the cutting fluid ranged from 0.11 to 0.17 wt.%. Regression models for surface roughness and SL were developed, with determination coefficients of 61.65% and 81.64%, respectively.

Overall, the optimized process with NP additives offers significant quantitative benefits in terms of surface finish and time efficiency, making it a more cost-effective and productive option. When comparing the optimized milling parameters—920 rpm, 0.02 in depth of cut, and a feed rate of 10.5 in/min—the validation results with NP additives yielded an R_a of 764 nm and an SL of 1.6 kW, while without NP additives, the predicted results were R_a of 779 nm and SL of 1.85 kW. Although R_a remains within the acceptable range, the SL is reduced by 14%, which leads to lower operational expenses. The reduced spindle load directly lowers electricity costs, while the optimized surface finish minimizes the need for additional finishing operations, making the process more cost-effective and sustainable. In summary, the optimized parameters contribute to a more sustainable and cost-effective process by balancing cutting speed, surface quality, and energy consumption, while reducing secondary processing requirements.

Acknowledgements

Authors acknowledge the support from Universidad de Monterrey under Grant UIN19550 and to the company FRISA for providing equipment and materials for this research.

REFERENCES

[1] K. Holmberg and A. Erdemir, "Influence of tribology on global energy consumption, costs and emissions," *Friction*, vol. 5, no. 3, pp. 263–284, Sep. 2017, doi: 10.1007/s40544-017-0183-5.

[2] W. Cai, C. Liu, K. H. Lai, L. Li, J. Cunha, and L. Hu, "Energy performance certification in mechanical manufacturing industry: A review and analysis," *Energy Conversion and Management*, vol. 186, no. 15, pp. 415-432, Mar. 2019. doi: 10.1016/j.enconman.2019.02.041.

[3] A. K. Sharma, A. K. Tiwari, and A. R. Dixit, "Progress of Nanofluid Application in Machining: A Review," *Materials and Manufacturing Process*, vol. 30, no. 7, pp. 813–828, Oct. 2015, doi: 10.1080/10426914.2014.973583.

[4] A. P. Reverberi, D. M. D'Addona, A. A. G. Bruzzone, R. Teti, and B. Fabiano, "Nanotechnology in machining processes: Recent advances," *Procedia CIRP*, vol. 79, pp. 3–8, Jan. 2019, doi: 10.1016/j.procir.2019.02.002.

[5] L. Peña-Parás, D. Maldonado-Cortés, M. Rodríguez-Villalobos, A. Sauceda, I. J. Aguilar, J. A. Villanueva, P. A. Cárdenas "Nanoparticle lubricant additives applied in a CNC lathe ball screw component for improving the quality of machined workpieces: A case study," *Wear*, vol. 523, p. 204752, Jan. 2023, doi: 10.1016/j.wear.2023.204752.

[6] M. S. Najiha, M. M. Rahman, and K. Kadirgama, "Performance of water-based TiO_2 nanofluid during the minimum quantity lubrication machining of aluminium alloy, AA6061-T6," *Journal of Cleaner Production*, vol. 135, pp. 1623–1636, Jan. 2016, doi: 10.1016/j.jclepro.2015.12.015.

[7] N. Tosun, S. Rostam, and S. Raul, "Use of Nano Cutting Fluid in Machining," *Proceedings of the International Conference on Advances in Mechanical and Automation Engineering - MAE*, pp. 17–21, Aug. 2016, doi: 10.15224/978-1-63248-102-3-43.

[8] T. Bakalova, L. Svobodová, P. Rosická, K. Borůvková, L. Voleský, and P. Louda, "The application potential of SiO_2, TiO_2 or Ag nanoparticles as fillers in machining process fluids," *Journal of Cleaner Production*, vol. 142, pp. 2237–2243, Nov. 20176, doi: 10.1016/j.jclepro.2016.11.054.

[9] N. Talib, R. M. Nasir, and E. A. Rahim, "Tribological behaviour of modified jatropha oil by mixing hexagonal boron nitride nanoparticles as a bio-based lubricant for machining processes," *Journal of Cleaner Production*, vol. 147, pp. 360–378, Jan. 2017, doi: 10.1016/j.jclepro.2017.01.086.

[10] G. E. García, F. Trigos, D. Maldonado-Cortés, and L. Peña-Parás, "Optimization of surface roughness on slitting knives by titanium dioxide nano particles as an additive in grinding lubricant," *International Journal of Advanced Manufacturing Technology*, vol. 96, no. 9–12, pp. 4111–4121, Mar. 2018, doi: 10.1007/s00170-018-1834-z.

[11] M. A. M. Ali, A. I. Azmi, M. N. Murad, M. Z. M. Zain, A. N. M. Khalil, and N. A. Shuaib, "Roles of new bio-based nanolubricants towards eco-friendly and improved machinability of Inconel 718 alloys," *Tribology International*, vol. 144, p. 106106, Dec. 2019, doi: 10.1016/j.triboint.2019.106106.

[12] L. Peña-Parás, J. A. Sánchez-Fernández, Cr. R. Martínez, J. A., Ontiveros, K. I. Saldívar, L. M. Urbina, M. J. Arias, P. García-Pineda, B. Castaños, "Evaluation of anti-wear properties of metalworking fluids enhanced with halloysite nanotubes," *Applied Sciences*, vol. 7, no. 10, pp. 1–15, Oct. 2017, doi: 10.3390/app7101019.

[13] L. Peña-Parás, D. Maldonado-Cortés, P. García, M. Irigoyen, J. Taha-Tijerina, and J. Guerra, "Tribological performance of halloysite clay nanotubes as green lubricant additives," *Wear*, vol. 376–377, pp. 885–892, Apr. 2017, doi: 10.1016/j.wear.2017.01.044.

[14] M. Zhang, Y. Qin, and G. Yang, "The anti-wear properties and tribofilm evolution of organically modified halloysite nanotubes," *Tribology International*, vol. 192, p. 109331, Jan. 2024, doi: 10.1016/j.triboint.2024.109331.

[15] P. Yuan, D. Tan, and F. Annabi-Bergaya, "Properties and applications of halloysite nanotubes: Recent research advances and future prospects," *Applied Clay Science*, vol. 112–113, pp. 75–93, May 2015, doi: 10.1016/j.clay.2015.05.001.

[16] B. Lecouvet, J. Horion, C. D'Haese, C. Bailly, and B. Nysten, "Elastic modulus of halloysite nanotubes," *Nanotechnology*, vol. 24, no. 10, p. 105704, Feb. 2013, doi: 10.1088/0957-4484/24/10/105704.

[17] D. Maldonado-Cortés et al., "Improvement of tribological properties through the application of laser surface texturing and nanolubricants in CNC equipment elements," *Tribology in Industry*, vol. 42, no. 1, pp. 159–164, Mar. 2020, doi: 10.24874/ti.2020.42.01.15.

[18] K. N. Mwangi, J. Wambua, F. M. Mwema, J. M. Wakiru, and T. C. Jen, "Evaluation of Surface Quality and Productivity in Conventional Milling of Copper Beryllium Using Minimum Quantity Lubrication," *Tribology in Industry*, vol. 46, no.3, pp. 355–367, Sep. 2024, doi: 10.24874/ti.1566.10.23.01.

[19] P. Karolczak, M. Kowalski, and K. Raszka, "The effect of the use of cutting zone minimum quantity lubrication and wiper geometry inserts on titanium Ti6Al4V surface quality after turning," *Tribology in Industry*, vol. 43, no. 2, pp. 321–333, Jun. 2021, doi: 10.24874/ti.1077.03.21.05.

[20] R. V. Rao, D. P. Rai, and J. Balic, "A multi-objective optimization of machining and micro-machining processes using non-dominated sorting teaching–learning-based optimization algorithm," *Engineering Applications of Artificial Intelligence*, vol. 29, no. 8, pp. 1715–1737, Mar. 2016, doi: 10.1007/s10845-016-1210-5.

[21] L. Peña-Parás, D. Maldonado-Cortés, M. Rodríguez-Villalobos, A. G. Romero-Cantú, O. E. Montemayor, M. Herrera, G. Trousselle, J. González, W. H., "Optimization of milling parameters of 1018 steel and nanoparticle additive concentration in cutting fluids for enhancing multi-response characteristics," *Wear*, vol. 426–427, no. January, pp. 877–886, Apr. 2019, doi: 10.1016/j.wear.2019.01.078.

[22] M. K. Gupta, P. K. K. Sood, and V. S. Sharma, "Optimization of machining parameters and cutting fluids during nano-fluid based minimum quantity lubrication turning of titanium alloy by using evolutionary techniques," *Journal of Cleaner Production*, vol. 135, pp. 1276–1288, Jun. 2016, doi: 10.1016/j.jclepro.2016.06.184.

[23] M. Kuntoğlu and H. Sağlam, "Investigation of progressive tool wear for determining of optimized machining parameters in turning," *Measurement*, vol. 140, pp. 427–436, Apr. 2019, doi: 10.1016/j.measurement.2019.04.022.

[24] G. Zhou, Q. Lu, Z. Xiao, C. Zhou, and C. Tian, "Cutting parameter optimization for machining operations considering carbon emissions," *Journal of Cleaner Production*, vol. 208, pp. 937-950, Oct. 2019, doi: 10.1016/j.jclepro.2018.10.191.

[25] C. Tian, G. Zhou, J. Zhang, and C. Zhang, "Optimization of cutting parameters considering tool wear conditions in low-carbon manufacturing environment," *Journal of Cleaner Production*, vol. 226, pp. 706–719, Apr. 2019, doi: 10.1016/j.jclepro.2019.04.113.

[26] P. Hema, K. JayaPadmavath, and B. Narayana Reddy, "*CNC machining of alloy steel 4130 and optimization of process parameters*," *International Journal of Technical Innovation in Modern Engineering & Science*, vol. 5, no. 2, pp. 295–303, 2019.

[27] P. Sivaiah and D. Chakradhar, "Modeling and optimization of sustainable manufacturing process in machining of 17-4 PH stainless steel," *Measurement*, vol. 134, pp. 142–152, Oct. 2018, doi: 10.1016/j.measurement.2018.10.067.

[28] M. Sayuti, A. A. D. D. Sarhan, and M. Hamdi, "An investigation of optimum SiO_2 nanolubrication parameters in end milling of aerospace Al6061-T6 alloy," *International Journal of Advanced Manufacturing Technology*, vol. 67, no. 1, pp. 833–849, Oct. 2012, doi: 10.1007/s00170-012-4527-z.

[29] K. N. Ronoh, N. W. Karuri, F. M. Mwema, H. T. Ngetha, S. A. Akinlabi, and E. T. Akinlabi, "Evaluation of the surface roughness of Ti-6Al-4V for surface grinding under different cooling methods using conventional and vegetable oil-based cutting fluids," *Tribology in Industry*, vol. 41, no. 4, pp. 634–647, Dec. 2019, doi: 10.24874/ti.2019.41.04.15.

[30] I. Veza, M. Spraggon, I. M. R. Fattah, and M. Idris, "Response surface methodology (RSM) for optimizing engine performance and emissions fueled with biofuel: Review of RSM for sustainability energy transition," *Results in Engineering*, vol. 18, no. Mar. 2023, doi: 10.1016/j.rineng.2023.101213.

[31] D. C. Montgomery, *Design and Analysis of Experiments*, 8th edition. John Wiley & Sons, Inc., 2013.

[32] A. K. Sharma *et al.*, "Novel uses of alumina/graphene hybrid nanoparticle additives for improved tribological properties of lubricant in turning operation," *Tribology International*, vol. 119, pp. 99–111,Nov. 2018, doi: 10.1016/j.triboint.2017.10.036.

[33] A. K. Sharma, R. K. Singh, A. R. Dixit, and A. K. Tiwari, "Novel uses of alumina-MoS_2 hybrid nanoparticle enriched cutting fluid in hard turning of AISI 304 steel," *Journal of Manufacturing Process*, vol. 30, pp. 467–482, Oct. 2017, doi: 10.1016/j.jmapro.2017.10.016.

[34] N. S. Mohamad and S. Kasolang, "Optimized characterization of response surface methodology on lubricant with titanium oxide nanoparticles," *Industrial Lubrication and Tribology*, vol. 69, no. 3, pp. 387–392, Mar. 2017, doi: 10.1108/ILT-09-2016-0214.

[35] Vignesh Kumar, "Investigation on surface defect machining of AISI 4340 steel," *Materials Today: Proceeding*, vol. 66, pp. 1189–1195, Jan. 2022, doi: 10.1016/j.matpr.2022.05.001.

[36] E. T. Sifuentes, O. V. Kharissova, D. Maldonado-Cortés, L. Peña-Parás, R. Michalczewski, and B. I. Kharisov, "A comparison of tribological properties of nanolubricants containing carbon nanotori and additional additives," *Materials Chemistry and Physics*, vol. 272, p. 124973, Jun. 2021, doi: 10.1016/j.matchemphys.2021.124973.

[37] J. A. Ortega, M. A. Sayeed Biswas, M. M. Rahman, V. Martinez, L. Peña-Parás, and D. Maldonado-Cortés, "Investigating the lubrication performance of vegetable oils reinforced with HNT and MMT nanoclays as green lubricant additives," *Wear*, vol. 523, p. 204859, Mar. 2023, doi: 10.1016/j.wear.2023.204859.

[38] S. Kalpakjian and S. R. Schmid, Manufacturing Processes for Engineering. Pearson Education, 2016.